Mercaptophenol-Protected Gold Colloids as Nuclei for the Crystallization of Inorganic Minerals: Templated Crystallization on Curved Surfaces

J. Küther,[†] R. Seshadri,[†] G. Nelles,[‡] W. Assenmacher,[§] H.-J. Butt,[‡] W. Mader,[§] and W. Tremel*,[†]

Institut für Anorganische Chemie und Analytische Chemie, Johannes Gutenberg-Universität, Mainz, Becher Weg 24, D-55099 Mainz, Germany, Institut für Physikalische Chemie, Johannes Gutenberg-Universität, Mainz, Welder Weg 18, D-55099 Mainz, Germany, and Institut für Anorganische Chemie, Rheinische Friedrich Wilhelms-Universität, Bonn, Gerhard-Domagk-Strasse 1, D-53117 Bonn, Germany

Received December 3, 1998. Revised Manuscript Received January 15, 1999

The self-assembly of monolayers of thiols on gold(111) surfaces yields substrates that are able to template in a controlled manner, the nucleation and growth of crystals of calcium carbonate from solution. In the absence of additives, various factors such as the nature of the thiol, the temperature, and the pH are now established as influencing the nature and relative amounts of the different $CaCO_3$ phases (calcite, vaterite, and aragonite). Recently, we have been able to extend the use of thiol/gold self-assembled monolayers as templates for the growth of inorganic crystals by utilizing protected gold colloids instead of flat gold surfaces. The thiol monolayers that protect the colloids provide heterogeneous interfaces for the initial nucleation of the inorganic crystal. The utility of such a designer seeding is demonstrated through the crystallization of $CaCO_3$ in the calcite modification and $SrCO_3$ in the strontianite modification.

Introduction

It is perhaps instructive to draw a parallel between the structure of proteins and the real organization of inorganic materials in terms of the *hierarchy* of structure. In proteins, there are as many as four levels of organization. At the simplest level is the sequence of individual amino acids; this is the primary structure. These organize as helices or sheets to produce the secondary structure. The secondary structures can, in turn, organize to yield the tertiary and quaternary levels of the three-dimensional protein structure. In the realm of crystalline inorganic materials, there is at the simplest level the arrangement of atoms in the unit cell which decides the *phase*. The unit cells can be stacked along the different real-space directions, with the respective extents deciding the morphology and habits of the individual crystallites. The crystallites, in turn, organize into the real world of polycrystalline materials. This last level of organization might be seen as some sort of tertiary structure. Additional complexity arises when the inorganic crystals are arranged in some admixture with a matrix that could be organic. Combinations of crystallites of different phases are also sometimes found to be held together in a single matrix. As with the structures of proteins, at any level in the hierarchy, the structure is influenced by the organization at every lower level.

Compared with the sophistication reached in those branches of chemistry that deal with directed bonds, synthetic control over even the simplest level in the hierarchy of inorganic materials, viz., the contents of the unit cell, is in its infancy at the present time. Nevertheless, in recent years, considerable effort has been directed toward obtaining insights into and control over the other (higher) levels in the hierarchy.[1] In the effort to make highly organized inorganic materials, the imperative is provided from the natural world.[2,3] Examples abound in nature of systems that are able to achieve control over all levels of organization of inorganic materials: control over the crystalline phase, over the size and morphology of the individual crystallite, over the manner in which the individual crystallites are organized within a single matrix, etc.[4,5] Exemplary in this respect is the formation of pearls. Implanting flat inorganic surfaces between the mantle and shell of the red abalone switches the deposition of $CaCO_3$ from the usual nacreous aragonite to calcite. In the later stages

* Author to whom correspondence should be addressed.
[†] Institut für Anorganische Chemie und Analytische Chemie, Johannes Gutenberg-Universität, Mainz.
[‡] Institut für Physikalische Chemie, Johannes Gutenberg-Universität, Mainz.
[§] Rheinische Friedrich Wilhelms-Universität, Bonn.

(1) Mann, S. *J. Mater. Chem.* **1995**, *5*, 935.
(2) Heuer, A. H.; Fink, D. J.; Laraia, V. J.; Arias, J. L.; Calvert, P. D.; Kendall, K.; Messing, G. L.; Blackwell, J.; Rieke, P. C.; Thompson, D. H.; Wheeler, A. P.; Veis, A.; Caplan, A. I. *Science* **1992**, *255*, 1098.
(3) Bianconi, P. A. In *Materials Chemistry, An Emerging Discipline*; Interrante, L. V., Caspar, L. A., Ellis, A. B., Eds.; *ACS Advances in Chemistry Series 245*; American Chemical Society: Washington, 1995.
(4) Lowenstam, H. A.; Weiner, S. *On Biomineralization*; Oxford University Press: New York, 1989.
(5) Mann, S., Webb, J., Williams, R. J. P., Eds. *Biomineralization*; VCH: Weinheim, Germany, 1989.

10.1021/cm980773a CCC: $18.00
Published on Web 04/29/1999

of deposition, there is another switch back to aragonite. Both the calcite and the aragonite phases grow in a highly oriented manner, with the initial deposition being controlled by organic (usually protein) networks.[6]

In a seminal paper, Mann[7] has established the utility of organic−inorganic interfaces in controlling nucleation and growth of crystals. He points out that at the level of ions interacting with the organic groups that are exposed to the solution (or other phase from which growth takes place) *epitaxy* between the growing crystal and the organic surface is only secondary to the templating effect provided by an interface in an otherwise homogeneous medium. Much of the recent work in attempting to control the different levels of organization of inorganic materials has involved the use of organic interfaces in various manifestations: as molecules (such as proteins) coated on glass slides,[8] as micelles or bicontinuous emulsions,[1,9,10] as Langmuir monolayers at the air−water interface,[11] as gels,[12] as self-assembled monolayers (SAMs),[13] etc. The organic interface that we have been using as crystallization templates for calcium and strontium carbonates[14−16] are SAMs of alkyl thiols on gold(111) surfaces.[17] We have been guided in this choice for the following reasons: the thiols are easily made, relatively stable, and simple to deposit (self-assemble). In addition, surface plasmon spectroscopy (SPS) provides a convenient and powerful tool to investigate the assembly and modification of thiols on gold-coated glass substrates.[18] Finally, access to the surface structure through atomic force microscopy (AFM) is possible,[19] allowing the establishment of epitaxy, when present, between the substrate and the templated crystal. During the course of these studies we have additionally found that the ability of gold to conduct charge is conductive to the deposition of ions. Thus, even on an "inert" surface such as gold(111) coated with a hexadecanethiol SAM, more crystals of calcium carbonate deposit than on a clean glass surface under identical conditions. This has also been observed in experiments in our lab involving the deposition of iron oxide−hydroxides on SAM surfaces.[20] The SAM surfaces can be modified through the organic functionality at the end of the molecule, usually the ω functionality on a long-chain thiol. Through this, there is some control over polarity, structure, and even specific chemical recognition by the SAM. Using dithiol SAMs, one can further attach gold colloids to the SAM surface, thereby achieving a microscopic roughening of the surface.[21] This increases the number of nucleation sites.

Are we obliged to limit the templating effects of organic monolayers on gold to surfaces that are flat? The answer is no. In recent years, the chemistry of thiol SAMs on gold surfaces has been extended to gold colloids. Protecting gold colloids (of diameters less than 10 nm) with thiols yields the possibility to form stable nanoparticles that in many ways behave like molecules.[22−25] For instance, such protected colloids can form *solutions* rather than *sols* that are stable in the absence of dispersing agents. These colloidal particles can be precipitated and redissolved. The solvent can be evaporated and the solid colloidal powders collected. Attempting this with the more traditional colloidal sols would yield particles of bulk gold that would not redisperse. Importantly, because these colloidal particles are small, the surface area of gold that is accessible to the thiol is significant. Thus, typical solution concentrations are sufficient that NMR spectra in solution can be recorded. Recording IR spectra in transmission from powders of the thiol-protected colloids is also feasible. This enhances our ability to perform many steps in the chemical modification of the thiols fixed to gold colloids with sufficient characterization at every step. Recently, we have used this aspect of the SAM chemistry of protected colloids to tether through a functionalized alkyl thiol, a Ru(III) ring-opening metathesis polymerization catalyst.[26] This has resulted in a catalytic system that bridges homogeneous and heterogeneous behavior. This nearly molecular behavior of thiol-protected colloids should not detract from the fact that they possess a surface that is mostly close packed (111), being the faces of cuboctahedra or multiply-twinned pairs (MTP) of cuboctahedra. It should, therefore, be possible to extend the templating ability of SAMs on *flat* gold surfaces to SAMs on colloid surfaces. We have found that this is indeed true and made a communication to this end.[27] Because of the form that most of the crystallite assemblies adopt, we refer to the crystallization products as spherules. Going from gold−glass surfaces to colloids in solution introduces some interesting new aspects. First, the crystallization is carried out heterogeneously (at an interface) from a homogeneous solution. Second, in terms of the topology of the template, we have made the transition from two-dimensional Euclidean space E^2 to the curved two-dimensional space S^2. For reasons that we will explain, crystallite−crystallite interactions be-

(6) Fritz, M.; Belcher, A. M.; Radmacher, M.; Walters, D. A.; Hansma, P. K. Stucky, G. D.; Morse, D. E.; Mann, S. *Nature* **1994**, *371*, 49. Zaremba, C. M.; Belcher, A. M.; Fritz, M.; Li, Y.; Mann, S.; Hansma, P. K.; Morse, D. E.; Speck, J. S.; Stucky, G. D. *Chem. Mater.* **1996**, *8*, 679.

(7) Mann, S. *Struct. Bonding* **1983**, *54*, 125.

(8) Weiner, S.; Addadi, L. *J. Mater. Chem.* **1997**, *7*, 689.

(9) Walsh, D.; Mann, S. *Adv. Mater.* **1997**, *9*, 658.

(10) Mann, S.; Burkett, S. L.; Davis, S. A.; Fowler, C. E.; Mendelson, N. H.; Sims, S. D.; Walsh, D.; Whilton, N. T. *Chem. Mater.* **1997**, *9*, 2300.

(11) Jacquemain, D.; Wolf, S. G.; Leveiller, F.; Deutsch, M.; Kjaer, K.; Als-Nielsen, J.; Lahav, M.; Lieserowitz, L. *Angew. Chem., Int. Ed. Engl.* **1992**, *31*, 130.

(12) Busch, S.; Kniep, R. *Angew. Chem.* **1996**, *108*, 2787.

(13) Archibald, D. D.; Quadri, S. B.; Gaber, B. P. *Langmuir* **1996**, *12*, 538.

(14) Küther, J.; Tremel, W. *J. Chem. Soc., Chem. Commun.* **1997**, 2029.

(15) Küther, J.; Seshadri, R.; Knoll, W.; Tremel, W. *J. Mater. Chem.* **1998**, *8*, 641.

(16) Küther, J.; Nelles, G.; Seshadri, R.; Schaub, M.; Butt, H.-J.; Tremel, W. *Chem. Eur. J.* **1998**, *4*, 1834.

(17) Ulman, A. *Chem. Rev.* **1996**, *96*, 1533.

(18) Spinke, J.; Liley, M.; Schmitt, F. J.; Guder, H. J.; Angermaier, L.; Knoll, W. *J. Chem. Phys.* **1993**, *99*, 7012.

(19) Nelles, G.; Schönherr, H.; Jaschke, M.; Wolf, H.; Schaub, M.; Küther, J.; Tremel, W.; Bamberg, E.; Ringsdorf, H.; Butt, H.-J. *Langmuir* **1998**, *14*, 808.

(20) Nagtegaal, M.; Tremel, W. Unpublished results.

(21) Küther, J.; Seshadri, R.; Nelles, G.; Butt, H.-J.; Knoll, W.; Tremel, W. *Adv. Mater.* **1998**, *10*, 401.

(22) Brust, M.; Walker, M.; Bethell, D.; Schiffrin, D. J.; Whymann, R. *J. Chem. Soc., Chem. Commun.* **1994**, 801.

(23) Brust, M.; Fink, J.; Bethell, D.; Schiffrin, D. J.; Kiely, C. *J. Chem. Soc., Chem. Commun.* **1995**, 1655.

(24) Whetten, R. L.; Khoury, J. T.; Alvarez, M. M.; Murthy, S.; Vezmar, I.; Wang, Z. L.; Stephens, P. W.; Cleveland, C. L.; Luedtke, W. D.; Landmann, U. *Adv. Mater.* **1996**, *8*, 428.

(25) Badia, A. L.; Singh, S.; Demers, L.; Cuccia, L.; Brown, G. R.; Lennox, R. B. *Chem. Eur. J.* **1996**, *2*, 359.

(26) Bartz, M.; Küther, J.; Seshadri, R.; Tremel, W. *Angew. Chem.* **1998**, *110*, 2646.

(27) Küther, J.; Seshadri, R.; Tremel, W. *Angew. Chem.* **1998**, *110*, 3196.

come at least as important as the crystallite−surface interactions.

We have recently become aware of work by Heywood and co-workers on the use of hyperbranched polymers with suitable terminal substitutions for the nucleation of calcium carbonate in solution. Through use of hyperbranched polymers with different generations of branching, the spacings between the groups at the termini can be controlled. This has allowed these authors to selectively crystallize the three different modifications of calcium carbonate.[28]

In this contribution, we employ *p*-mercaptophenol to form SAMs on gold-coated glass slides. These are used to template the deposition of calcium carbonate from solution. We then use this thiol to protect (through the formation of SAMs) gold colloids with diameters of around 3 nm. The protected colloids are soluble in water provided the pH is raised above 12.[23] Calcium and strontium carbonates are then precipitated from these colloidal solutions, with the protected colloids acting as seeds for the crystallization process. We see no reason why the formation of such spherules should be restricted to carbonates of calcium or strontium. Suggestions for future work are made.

Experimental Section

p-Mercaptophenol was purchased from Aldrich and used as obtained. Gold colloids were prepared following the method of Brust[22,23] in two-phase toluene−water systems, using tetraoctylammonium bromide to transfer chloroauric acid from water to toluene and then reducing the Au(III) to Au(0) at the water−toluene interface using aqueous $NaBH_4$. The addition of *p*-mercaptophenol results in the colloids being precipitated. Typically 0.5 g (4 mM) of the thiol was added to a 50 mL batch of the colloidal sol in toluene containing 0.1 g (0.5 mM) of Au. The precipitated powders could be washed with toluene and dichloromethane and easily redissolved in alcohols. The powders were also soluble in water provided the pH was raised to greater than 12. It is specifically for its solubility behavior that this thiol was chosen. The distinction between solution and dispersion is an important one for the purposes of this work and should be noted. The colloidal particles dissolve in suitable solvents without there being a need to sonicate, agitate, etc. These solutions are stable for weeks (albeit slightly light-sensitive) in the absence of any extraneous stabilizing agent.

Gold-coated glass substrates were prepared by evaporation in a Balzers BAE250 vacuum coating unit under pressures of less than 5×10^{-6} hPa, typically depositing 48 nm of gold after first depositing 2 nm of Cr as an adhesive buffer layer. The metal deposition was monitored in situ using a quartz crystal oscillator. These substrates were placed for 12 h in 1 mM solutions of *p*-mercaptophenol in ethanol before the crystallization experiments.

Transmission, electron microscopy (TEM) was performed on a Philips CM300UT FEG operating at 300 kV and equipped with a EDS system (Noran Voyager, Ge detector). The images were acquired with a retractable 2000 × 2000 CCD (Gatan MSC). Spotting ethanolic solutions of the colloids on the TEM grids resulted in agglomerates of material. Instead, the thiophenol-coated colloids were prepared on carbon-coated copper grids through direct dispersion of the powders.

AFM measurements on the colloids in tapping mode were made on a Digital Instruments Nanoscope IIIa microscope using Si cantilevers (resonance frequencies typically of around 250 kHz). The samples of the thiophenol-coated colloids were dissolved in 2-propanol and spin-cast onto freshly cleaved mica substrates.

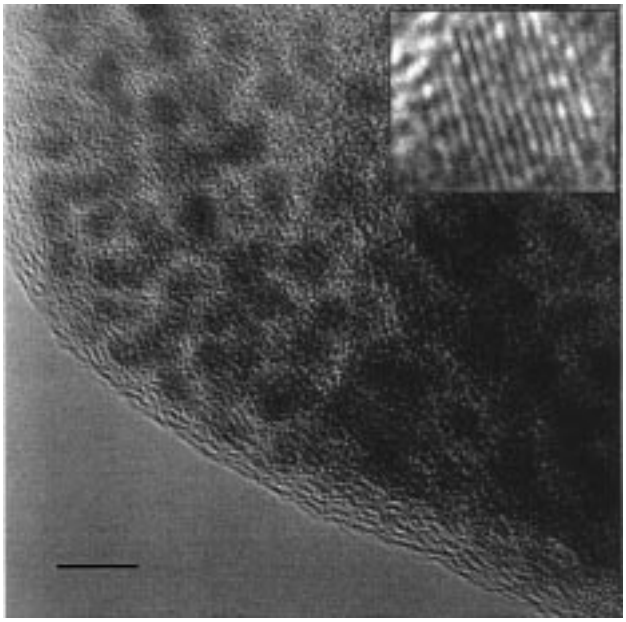

Figure 1. High-resolution transmission electron micrographs of the *p*-mercaptophenol-coated colloidal gold particles. The bar is 5 nm. The inset shows the (111) lattice fringes of an isolated particle about 0.35 nm apart.

For scanning electron microscopy of the crystallization products, a Zeiss DSM 962 instrument operating between 5 and 15 keV was employed. The samples were sputtered with gold before the measurements. Powder X-ray diffraction profiles were recorded in transmission with samples held between Scotch tape. In the case of the crystallization experiments carried out on the flat substrates, the samples had to be scraped off from the substrate. For the material collected after crystallization on the colloidal seeds, no further manipulation was required. A Siemens D5000 diffractometer was used for this prpose. The data were collected with monochromatized Cu $K\alpha_1$ radiation (1.540 56 Å) by step scanning with steps of 0.02° between 20° and 60° 2θ counting for 25 s/step. Data were subject to Rietveld analysis[29] as implemented in the XND program.[30]

The crystallization experiments were carried out in closed desiccators holding pH-adjusted (with aqueous NaOH) solutions of $CaCl_2$ or $SrCl_2$ (10 mM) in the presence or absence of different concentrations of colloids. CO_2 was allowed to diffuse into the solutions from the decomposition of solid ammonium carbonate which was also placed in the desiccator. The temperature at which the crystallizations were carried out was controlled by placing the whole desiccator in an oven, a refrigerator, or in the laboratory ambient. For crystallization on the SAMs on gold-coated glass slides, the slides were held with the active (SAM) surface downward in the solution. This prevents crystals nucleated in the solution from falling and collecting on the active surfaces. For crystallization on the protected colloid surfaces, witness glass slides were placed at the bottom of the dishes containing homogeneous solutions containing $CaCl_2$ (or $SrCl_2$) and the colloids. The products collected on these glass slides were used for further analysis. In both cases, crystallizations were arrested after 24−48 h and the slides removed and blown dry in a gentle stream of nitrogen.

Results and Discussion

Characterization of the Protected Colloidal Particles. Figure 1 displays high-resolution transmission electron micrographs of *p*-mercaptophenol-protected

(28) Heywood, B. R.; et al. Presented at the 1st International Conference on Inorganic Materials, Versailles, France, Sept 1998.

(29) Rietveld, H. M. *J. Appl. Crystallogr.* **1969**, *2*, 65.
(30) Bérar, J.-F.; Garnier, P. *NIST Special Publ.* **1992**, *846*, 212.

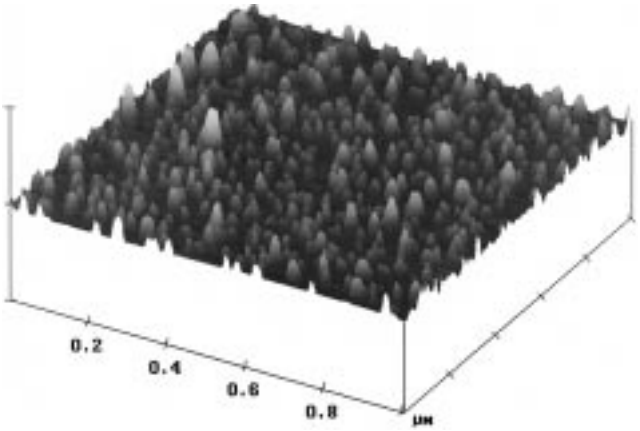

Figure 2. Tapping mode atomic force micrograph of the *p*-mercaptophenol-coated gold colloids spin-cast on a mica surface. The small humps are isolated particles, and the larger ones are clusters or aggregates of more than one particle. The tick marks along the *z* direction correspond to 30 nm.

colloidal gold particles. We find the particles have diameters of around 3 nm. Energy-dispersive X-ray spectra of areas with gold particles show Au as well as S and C signals. The contrast of the Au colloids seems to be affected by the protection layer of the thiophenol. In high resolution, the (111) lattice fringes of Au are visible in the colloidal particle that is shown in the inset. At this magnification, some facetting of the particle is observed. To our surprise, all of the particles seem to be single-crystalline rather than twinned. Usually small, colloidal gold particles when prepared in aqueous solutions in the absence of protecting agents display multiple twinning of cuboctahedral crystals.[31] The protection layer of the thiol stabilizes the dangling bonds on the Au surface. This could decrease the need for the individual crystals to reduce the area of high-energy surfaces through twinning.

When solutions of the *p*-mercaptophenol-protected colloidal gold particles are spin-cast on mica and examined in the atomic force microscope, they are seen to be isolated or clustered in spherical aggregates. This is shown in Figure 2 as an AFM surface plot. Considering the TEM micrographs, we would expect the particles to show some uniformity in their sizes. The AFM images bear this out. From AFM measurements, estimates of particle size are generally not as reliable as those obtained from electron microscopy, particularly when the particles are not close-packed and when particle dimensions might be of the order or smaller than the dimensions of the AFM tip. Nonetheless, the dimensions we obtain are consistent with the sizes observed in the electron micrographs. We have found in the course of these studies that the nature of the aggregates formed on spin-casting colloids is strongly dependent on the thiol that is used to protect the colloid. The different thiols are possessed of different degrees of hydrophobicity and therefore interact with one another, the mica surface, and the evaporating solvent in distinct ways.

$CaCO_3$ Crystallization on Flat SAM−Gold Surfaces. Because of solubility constraints, we were obliged to perform the colloidal seeding at a pH value of 12. We

(31) Kirkland, A. I.; Edwards, P. P.; Jefferson, D. A.; Duff, D. G. *Annual Report C*; The Royal Society of Chemistry: Cambridge, U.K., 1988; pp 247−304.

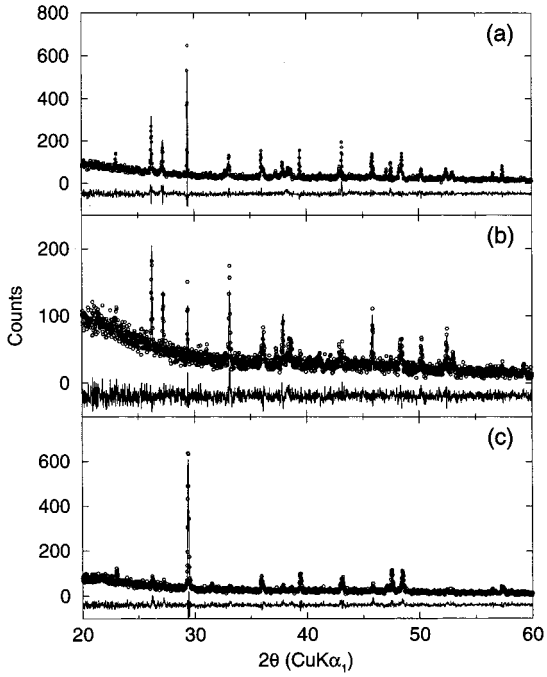

Figure 3. Experimental, Rietveld-fitted, and difference X-ray diffraction profiles of calcium carbonate collected after deposition on flat *p*-mercaptophenol SAM surfaces. The conditions at which the different $CaCO_3$ samples were produced are (a) 22 °C and pH 10, (b) 45 °C and pH 10, and (c) 22 °C and pH 12. The patterns in panels a and b are two-phase fits to the structures of calcite and aragonite. Panel c corresponds to a fit to calcite alone.

therefore start by comparing the nature of the $CaCO_3$ phases formed on the *p*-mercaptophenol SAMs on flat gold surfaces at pH = 10 and 12. In Figure 3, we display the experimental and fitted powder XRD profiles corresponding to the material collected from the flat *p*-mercaptophenol SAM after crystallization at (a) 22 °C and pH = 10, (b) 45 °C and pH 10, and (c) 22 °C and pH = 12. In the first two cases, both the calcite and aragonite phases of $CaCO_3$ were refined. From the Rietveld scale factors, it is possible to obtain the relative amounts of the different phases. From such an analysis, we find that, at 22 °C and pH 10, the weight fractions of calcite and aragonite formed on the *p*-mercaptophenol SAM surface are in the ratio of 40:60. At the same pH but at 45 °C the calcite−aragonite ratio is found to be 14:86 in keeping with results that we have on other SAM surfaces, that increasing temperatures favor aragonite.[14] The amount of aragonite formed at 22 °C on this surface is exceptionally high.[15] We examine possible reasons for this presently. These high aragonite amounts were promising for attempting the crystallization of spheroidal (perhaps spherulitic) aragonite assemblies around the colloidal nuclei. However, when the pH is raised to 12 (as necessitated for dissolving the protected colloids), the sole $CaCO_3$ phase formed is calcite, as seen in panel c of this figure. At the outset, it is therefore clear that colloidal templating under the conditions used here would not yield aragonite.

Figure 4 displays electron micrographs of the SAM surfaces with $CaCO_3$ crystals grown thereon, after crystallization experiments carried out at (a) 22 and (b) 45 °C. The initial pH was 10. Even at 22 °C, in contrast to our experience with other SAM surfaces,[15] there is a rather high amount of aragonite, seen as small ef-

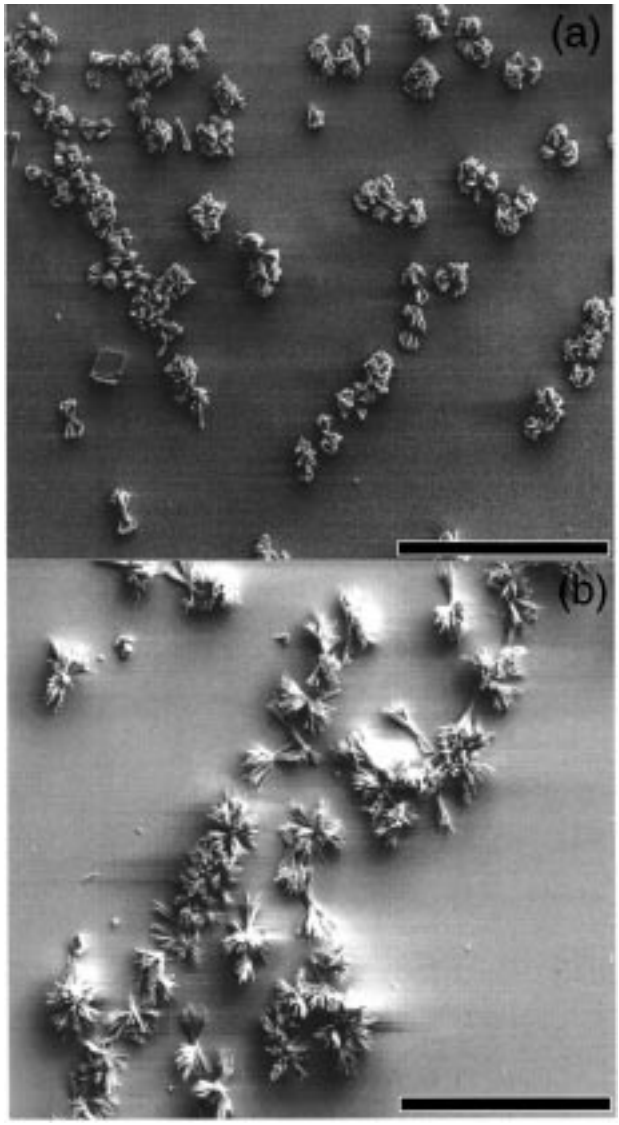

Figure 4. Scanning electron micrographs of the products obtained after crystallization of $CaCO_3$ on *p*-mercaptophenol SAM surfaces at pH 10. The temperatures were (a) 22 and (b) 45 °C. Rhombs of calcite and bundled needles of aragonite are observed in both micrographs. The scale bars correspond to 200 μm.

florescent bundles of needles. Because calcite forms relatively large and dense crystals, the weight fraction of calcite as obtained from X-ray profile analysis can be significant, even if only a few crystals are seen in the scanning electron micrographs. At 45 °C (panel b) the conditions are such that aragonite is strongly favored, consistent with the calcite−aragonite ratio of 14:86 obtained from the X-ray profiles. While the aggregates of the aragonite needles seem to form rather uniformly on the surface, there is no clear pattern of templating, with the bundles of needles (each needle being a trilling of aragonite single crystals) being oriented in a nonuniform way. This is to be contrasted to previous work from this laboratory where we have shown that provided the SAM can be constructed from thiols that organize in 2D lattices with lattice parameters commensurate with the lattice parameters of aragonite, evidence for epitaxial growth of aragonite can be obtained.[16] In that case also, the needles of aragonite are organized in efflorescent bundles, but the orientations are very uniform. Similar work involving crystallization under Langmuir monolayers of specific amphiphiles has been presented by Litvin et al.[32]

The question then is, why is the *p*-mercaptophenol SAM surface so suited for inducing the growth of aragonite rather than calcite? Clues could be obtained from the 2D structure of the SAM formed by *p*-mercaptophenol. Unfortunately, our attempts by AFM to obtain images of such structures have failed. Normally, the 2D crystalline structure of acidic SAM surfaces, such as those formed by ω-carboxylic acids on long-chain thiols, can be imaged in contact mode AFM in a liquid cell provided the strong Coulombic interactions that exist between the AFM tip and the SAM surface are screened through raising the ionic strength.[19] In the case of the *p*-mercaptophenol SAM, this has not proved possible.

In our previous work, we have noted that aragonite has a propensity for ill-formed SAM surfaces such as those assembled from thiols with short alkyl chains. On such ill-formed surfaces, it is possible that aragonite is rapidly nucleated, resulting in it being kinetically stabilized. On the *p*-mercaptophenol surface, no vaterite is observed. This is again in keeping with our earlier observations that vaterite and aragonite are complementary, and finding the one is invariably at the expense of finding the other.

We have observed in the X-ray patterns that when the initial pH at which the crystallization is carried out is raised to between 12 and 13, the only phase that forms is calcite. In Figure 5, the nature of the calcite crystals formed on flat *p*-mercaptophenol SAM surfaces under these conditions of higher pH is displayed. The scanning electron micrographs in panels a and b, acquired under different magnification conditions, show that the crystals form with a highly inhibited morphology. The likely reason for such inhibition is that, under the higher pH conditions, the phenolic OH groups that face outward into the solutions from which crystallization is carried out are ionized. Such inhibition is not very important when crystallizations are carried out on colloidal templates, as we shall see shortly.

$CaCO_3$ Crystallization around Protected Colloid Seeds. For the crystallization around the protected colloids, the parameters that were varied were the concentration of seed nuclei and the temperature at which the crystallizations were carried out. In all cases, the initial deep-pink solutions of protected gold colloids turned completely colorless at the end of the crystallization, from which we could conclude that the precipitation of $CaCO_3$ in some way resulted in an entrapment of the colloids. Indeed, the crystallization resulted in a grayish-black product that deposited at the bottom of the vessel onto the witness glass slides. Under all of the conditions of temperature and seed concentration employed by us, X-ray diffraction on the powders that were collected showed no evidence for any phase other than calcite. Typical examples of products obtained after crystallization are shown in the panels of Figure 6 after using a seed concentration of 10 mg of colloids/100 mL of solution and carrying out the crystallization at 22 °C. The micrographs shown here should be compared with

(32) Litvin, A. L.; Valiyaveettil, S.; Kaplan, D. L.; Mann, S. *Adv. Mater.* **1997**, *9*, 124.

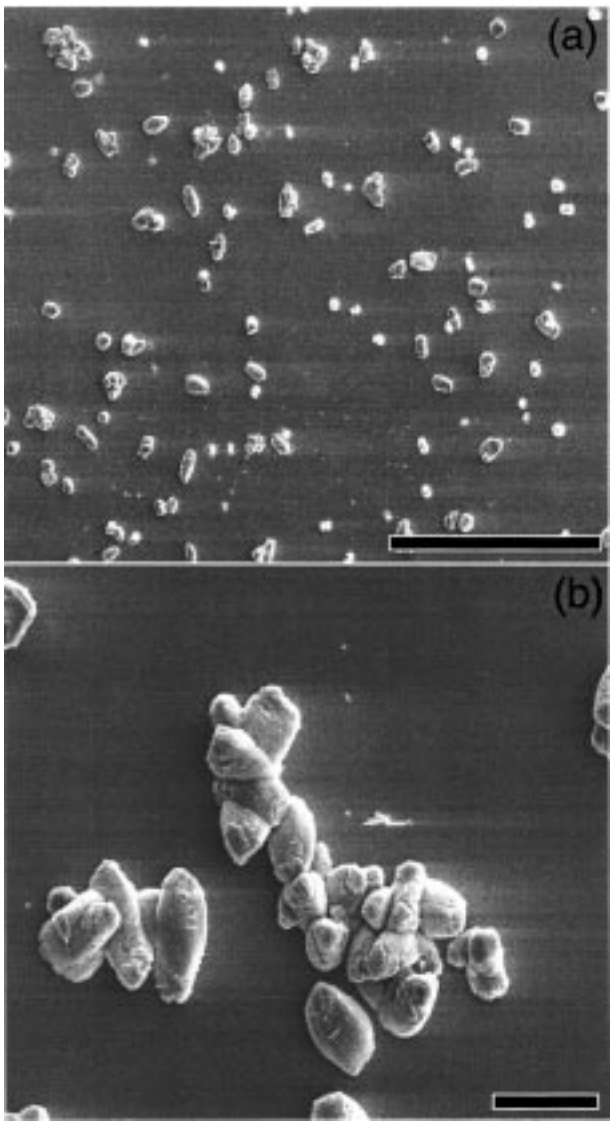

Figure 5. Scanning electron micrographs of the products obtained after crystallization of $CaCO_3$ on *p*-mercaptophenol SAM surfaces at pH 12 and 22 °C. Only calcite is obtained, and the crystallization is inhibited in terms of both the poor nucleation density of crystals and the morphologies of the crystals. The scale bars correspond to (a) 200 and (b) 20 μm.

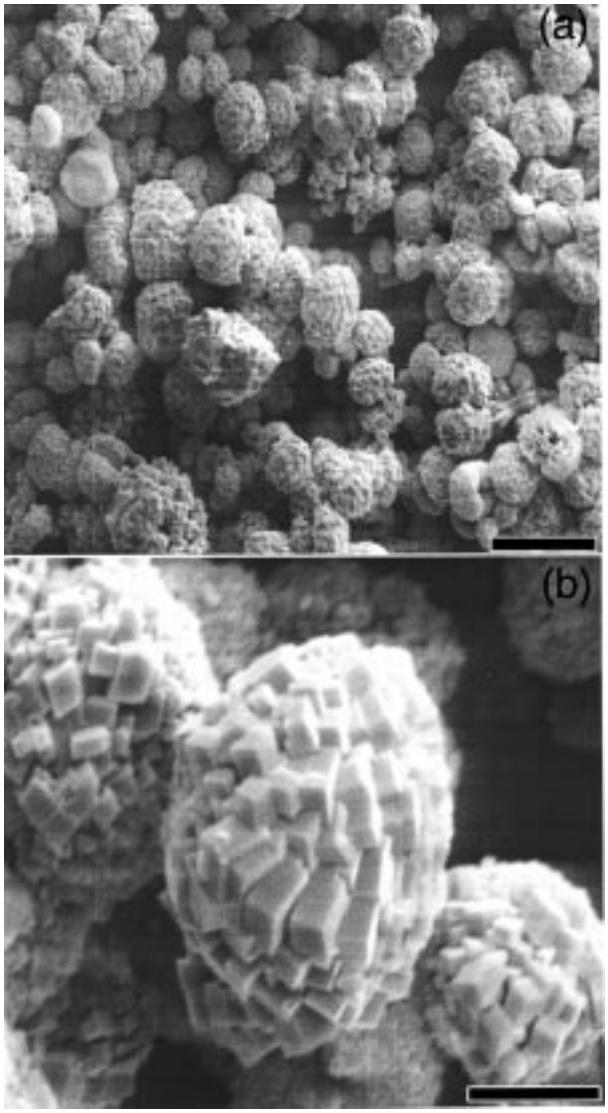

Figure 6. Scanning electron micrographs of the products obtained after crystallization of $CaCO_3$ around *p*-mercaptophenol-coated gold colloid seeds. The conditions were pH 12 and 22 °C, with a seed concentration of 10 mg/100 mL of solvent. The scale bars correspond to (a) 20 and (b) 5 μm.

micrographs of calcium carbonate crystals precipitated from solutions in the absence of gold colloids[27] under identical conditions. The morphologies of the calcite crystals so obtained are facetted and rhombohedral with slightly damaged edges. The products grown in the presence of gold colloids displayed in panel a, on the other hand, are spheroidal, suggesting our use of the term spherule. Typical spherules have diameters of around 10 μm. Some of these spherules are seen in higher magnification to have well-defined surfaces displaying complex aggregates of facetted calcite crystals. The crystals seem to organize radially, with the direction of growth being the body diagonal of the rhombohedral crystals or crystallographic [001]. The spherules have diameters (around $\sim$5 μm) of about 3 orders of magnitude larger than the diameters of the colloidal seeds (around $\sim$3 nm) that we believe nucleate the growth of the crystallite assemblies. It is quite possible, therefore, that the spherules contain within them more than a single colloidal seed. Certainly, the number of such spheroidal crystallite assemblies that we obtain are far fewer than the number of seed crystals that we use. We note that not all of the spherules are formed from such facetted crystals; a number of them have a much smoother surface. To find out whether the facetted structure is maintained even within the spherules, we have attempted to crush the assemblies before performing the microscopy. The resulting micrographs are displayed in the panels of Figure 7. Unfortunately, pressure seems to damage the facetting as seen from panel a. One cannot, therefore, be sure that the absence of facetting within the cleaved assembly is intrinsic or arises from the act of breaking the spherule.

The spheroidal nature of the crystallite assemblies would suggest that nucleation as well as the greater part of crystal growth takes place while the seeds are still in solution. Were some of the growth to take place after the assemblies had settled, the spherules might not be as equiaxed as we find them. Assuming that the spherules start to precipitate only after much of the Ca is depleted in the solution, it is possible that the growth

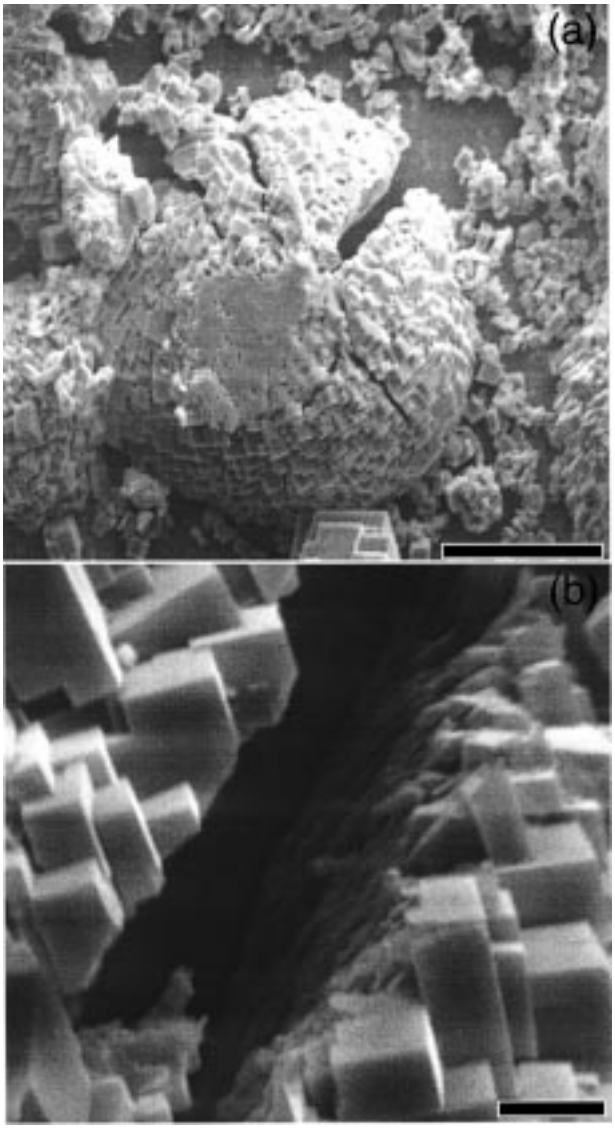

Figure 7. Attempts to examine the nature of one of the spherules by crushing them result in the crystals on the surface of the spherule being damaged (a). The insides (b) of the spherule do not look as crystalline (are not composed of facetted crystals) as the surface. The scale bars correspond to (a) 20 and (b) 2 μm.

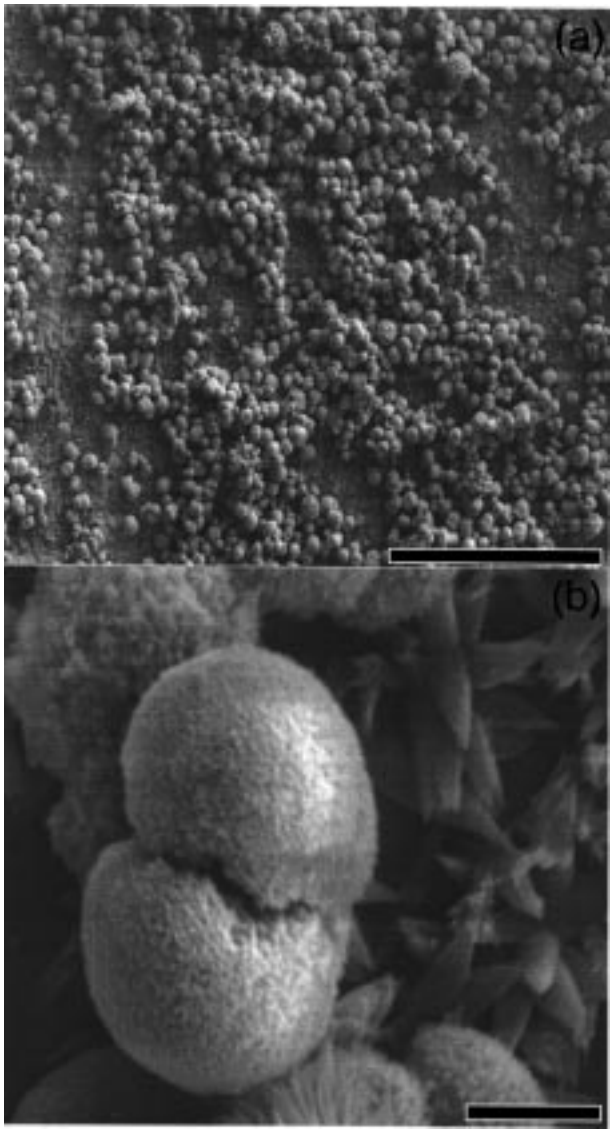

Figure 8. Scanning electron micrographs of the products obtained after crystallization of $CaCO_3$ around *p*-mercaptophenol-coated gold colloid seeds. The conditions were pH 12 and 4 °C, with a seed concentration of 10 mg/100 mL of solvent. Despite rather fluffy morphology; X-ray diffraction indicates only calcite. The scale bars correspond to (a) 200 and (b) 5 μm.

of facetted crystals takes place only in the later stages of the crystallization when the level of supersaturation is low and the crystals grow more slowly.

Further insight into the growth process is obtained from growing the calcite spherules at different temperatures and seed concentrations. We illustrate this with the micrographs in Figure 8. The conditions of crystallization were 4 °C and a seed concentration of 10 mg of colloids/100 mL of solution. The crystallite assemblies remain spheroidal but in higher magnification display a complete lack of facetting, being rather fluffy instead. Despite the morphology, the spherules seem to be composed purely of calcite, as verified by X-ray diffraction. The diffraction profiles for the spherules obtained at the lower temperatures are broader than those obtained from the products crystallized at 22 °C pointing to poorly crystallized material. The reason could be that, for a fixed Ca ion concentration, there is higher initial supersaturation at 4 °C, which results in rapid nucleation. The depletion of Ca in solution seems to take place at this stage so that there is insufficient Ca for the slow overgrowth of larger crystals.

$SrCO_3$ Crystallization around Protected Colloid Seeds. Because we were unable to obtain aragonite under the conditions of the crystallization around the protected colloid seeds, we were interested in simulating its seeding through crystallizing $SrCO_3$ instead. $SrCO_3$ almost always crystallizes as the mineral strontianite, which has a structure nearly identical to that of aragonite.[33] Indeed, because $SrCO_3$ is not plagued with problems of competing phases (unlike $CaCO_3$), its crystallization is useful to isolate important features in the crystallization of $CaCO_3$ including the establishment of epitaxy between the substrate and crystal when present.

The panels of Figure 9 display the products obtained after such seeded crystallization of strontianite. The

(33) Megaw, H. D. *Crystals Structures, A Working Approach*; W. B. Saunders: Philadelphia, 1973.

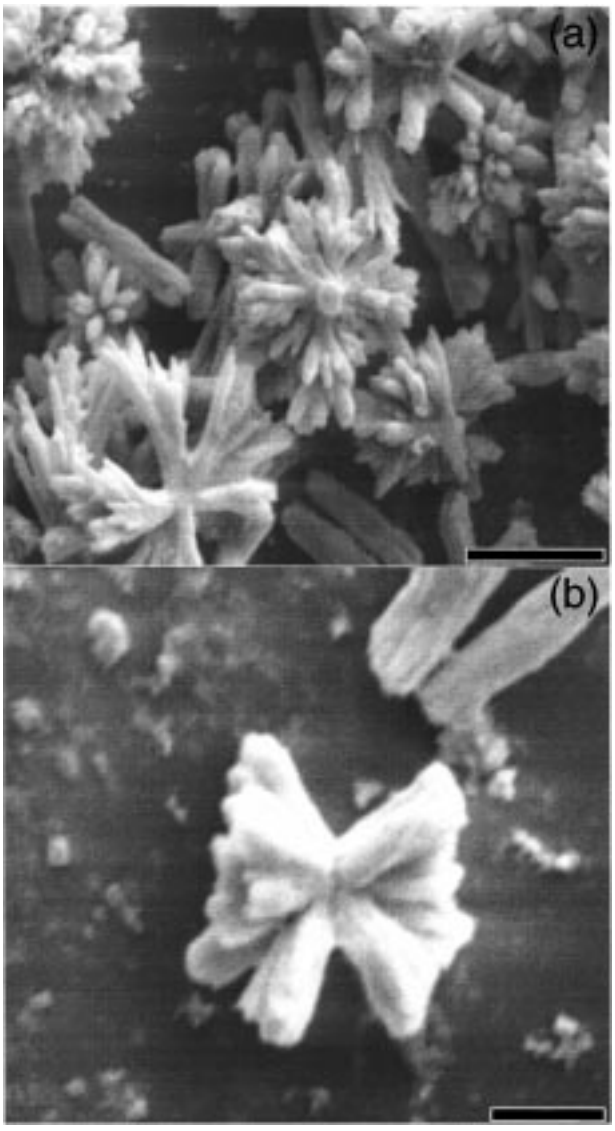

Figure 9. Scanning electron micrographs of the products obtained after crystallization of $SrCO_3$ in the strontianite modification around *p*-mercaptophenol-coated gold colloid seeds. The conditions were pH 12 and 4 °C, with a seed concentration of 10 mg/100 mL of solvent. The scale bars correspond to (a) 5 and (b) 2 μm. The smaller size of the assemblies of $SrCO_3$ crystals is a result of the higher initial supersaturation because of the smaller solubility product of $SrCO_3$.

conditions employed were a pH of 12 and a temperature of 4 °C. The seed concentration was 10 mg/100 mL of solvent. The usual morphology is needle-like, with each needle usually comprising a trilling of crystals with the long axis corresponding to crystallographic [001]. Again, at the rather high pH used, the needles are not as sharply facetted as they are under milder pH conditions. The presence of the colloidal seeds seems to induce the needles to cluster and grow out from a central point. This is actually the nature of the aragonite and strontianite bundles also when crystallization is carried out on flat surfaces; i.e., there is the tendency for many needles to grow out from a single point. However, because this single point in the present case is in an isotropic solution, the morphologies that can be obtained are quite different from what one finds on flat surfaces (cf. the micrographs in Figure 4b).

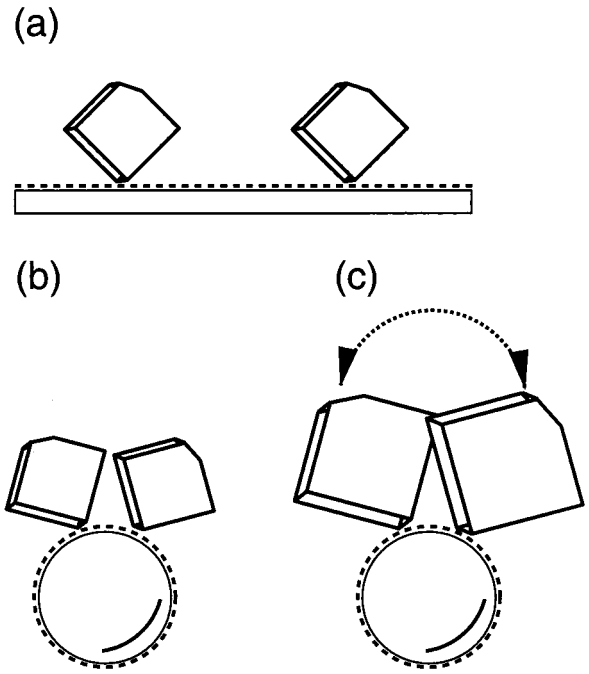

Figure 10. Scheme comparing the templated growth of crystals on (a) flat surfaces and (b and c) curved surfaces. When the crystals (or the aggregates) grow larger, crystal–crystal interactions become important and can simultaneously control and frustrate growth in the direction tangential to the seed particle.

Conclusions

The well-established function of organic interfaces in controlling the deposition and growth of inorganic materials provided us with the initial impetus to use self-assembled monolayers of ω-substituted alkylthiols on gold(111) surfaces for crystallizing calcium and strontium carbonates from solution. Recognizing that such interfaces are also possessed by protected gold colloids has permitted us to think of using them as crystallization seeds or templates. Results of such a crystallization have been demonstrated in this paper. The number of important inorganic materials that could be templated in the manner presented here are legion. We need to suitably choose thiols that simultaneously protect the colloid and are compatible with the solvent and the inorganic material. Comparing flat (Euclidean 2D or in the space E^2) templates with the colloid templates (which are curved 2D or in the space S^2), we observe significant differences in the nature of the crystallization products.

Some key issues here include:

(i) The ratio of atoms on the surface to those in the bulk for spherical objects scales approximately as the inverse diameter. For a given quantity of gold, the use of small colloids therefore maximizes the amount of heterogeneous surface on which templated crystallization can be carried out.

(ii) The crystallizations take place at an interface within completely *homogeneous* solutions and proceed for some time before the crystalline aggregates settle. This permits us to obtain crystalline aggregates with morphologies that are quite distinct from not only what are obtained on flat surfaces but also perhaps what *can* be obtained on flat surfaces.

(iii) An important issue in using a small, round template is that the crystals mutually frustrate the growth of one another in the direction tangential to the growing spherule. We attempt to depict such frustration in the scheme in Figure 10. The effect of this is that the morphology of the crystals formed at the later stages of growth around the spherical seed is strongly influenced by crystal−crystal interactions. This raises another interesting question that on the flat surface the number of crystals formed is far less than what is formed on the spherical seed template. We are unable to pinpoint a reason, but the ability of Coulombic repulsions to propagate over very large distances in 2D might play a role here. Indeed we often find that crystallizations on the 2D templates are along well-ordered lines on the surface.[16]

(iv) The quantities of material obtained from the crystallization around colloidal seeds are much larger. The use of seeds rather than flat surfaces allows us to obtain bulk products, i.e., powders.

(v) From the viewpoint of the topology of the colloidal seeds, comparisons can perhaps be drawn between crystallization around colloids and crystallization within a micelle.[10] The two template systems complement each other in the sense that in the one the growth is outward and in the other it is inward.

(vi) Assuming the thiophenol-coated colloids individually act as nuclei for the crystallization, their size (on the order of 3 nm) is small enough that they raise some interesting questions about how small heterogeneous nuclei need to be. These questions would be invalid in the present study were nucleation to be taking place around clusters of the colloids in solution instead of individual colloids. At the present time, we are unable to answer either question. An interesting future direction would be to attempt crystallizations around nuclei of different sizes. A related aspect is the use of different thiol protection groups. Neither of these parameters is easily varied without the solubility of the thiols in water being affected.

Acknowledgment. We thank Degussa, Hanau, for a generous gift of gold.

CM980773A